Energy Storage Materials 26 (2020) 371–377

Contents lists available at ScienceDirect

Energy Storage Materials

journal homepage: www.elsevier.com/locate/ensm

# Cu coated soft fabric as anode for lithium metal batteries

Luhan Ye [a,1], Peijian Feng [a,b,1], Xi Chen [a,1], Baohong Chen [a], Katrina Gonzalez [a], Jiahao Liu [b], In Kim [a,c], Xin Li [a,*]

[a] Harvard John A. Paulson School of Engineering and Applied Sciences, Harvard University, Cambridge, MA, 02138, USA
[b] Department of Polymer Science and Engineering, School of Chemistry and Chemical Engineering, Nanjing University, Nanjing, 210023, China
[c] Samsung SDI America, Inc, Auburn Hill, MI, 48326, USA

ARTICLE INFO

*Keywords:*
Lithium metal battery
Soft fabric
Cu coating

ABSTRACT

Lithium dendrite related problems form a major barrier that limits the application of lithium metal anode for Li-ion batteries. Here a copper coated 3D soft fabric anode was developed to show superior battery performance under an optimized mechanical stress for the lithium metal anode application. A scalable two-step dip-coating method was applied to coat Cu onto various insulating cloth fabrics, making them electrically conductive. In our battery tests, the 3D soft conductive fabric contributes to a more uniform lithium deposition during the battery cycling, which works for more than 1000 h. The mechanism for suppressing lithium dendrite growth by the mechanical interaction with 3D Cu-fabric was also revealed by a combination of microscopy characterization, electrochemical test and theoretical modeling, which provides the design principle for their future applications in lithium metal anode batteries.

## 1. Introduction

Lithium metal is considered as the ideal anode for future high-energy-density rechargeable batteries due to the high capacity of 3860 mA h/g and the low electrochemical potential of −3.040V versus the standard hydrogen electrode [1–4]. However, safety problems related to the lithium dendrite impede the application of lithium metal anode in lithium ion batteries [5]. The lithium dendrite formation may cause problems such as large volume change [6], depletion of liquid electrolyte [4], increased polarization, reduced Coulombic efficiency (CE) and even short-circuit induced explosion [7]. Numerous methods have been used to avoid Li dendrite growth in lithium metal batteries, including changing electrolyte solvents [8–11], using electrolyte additives [12–14], modifying lithium surface morphologies [15,16], utilizing solid electrolytes [17], synthesizing artificial solid electrolyte interfaces (SEI) [18–22], and so on [23–28].

3D substrate with well-designed structure is one promising method to prevent the dendrite growth. Many studies focused on the reduction and redistribution of local current density in 3D lithium anodes [29–31], which may mitigate the lithium dendrite growth caused by the heterogeneous nucleation during the plating and stripping processes [32]. Recently, Wang and co-workers demonstrated that the deposition of lithium metal on a soft substrate can relax the stress of dendrite formation by automatic wrinkling for a more uniform deposition of lithium and better battery performances [33]. This work suggests, in our opinion, the general importance of mechanical effect on controlling the lithium deposition in a soft substrate. In addition, there were evidences that applying certain external pressure to the battery operation can regulate the shape of lithium nucleation and give higher Coulombic efficiency [34–37]. Based on these previous works, we envision that there exist abundant mechano-electrochemical effects that can control the lithium deposition and dendrite growth behavior, understanding of which will be important to the design of more effective lithium metal battery systems.

Previously, we developed a two-step dip-coating method to coat Cu to the glass-fiber and other paper based insulting 3D substrates, making them electrically conductive for lithium metal anode applications [38]. Here copper coated 3D soft fabric (Cu-fabric) current collectors were for the first time developed by this method to show superior battery performances under an optimized mechanical stress for the lithium metal anode application. The role of the external pressure can be evaluated by cycling performance and scanning electron microscopy (SEM) imaging. By further modelling the dynamics of the lithium deposition, it was found that there exists an optimal external pressure for the cloth to hold the largest amount of lithium inside the pores of fabric. Such design principle

* Corresponding author.
*E-mail address:* lixin@seas.harvard.edu (X. Li).
[1] L. Ye, P. Feng, and X. Chen contributed equally to this work.

https://doi.org/10.1016/j.ensm.2019.11.007
Received 3 September 2019; Received in revised form 3 November 2019; Accepted 4 November 2019
Available online 9 November 2019

is directly applied to and confirmed by our experiments.

The Cu-fabric is first prepared by treating the cloth fiber with a two-step dip-coating method (Fig. 1a) [38,39], which is cost efficient and scalable. Combined with the further application of an optimal external pressure during battery operations, the 3D conductive fabric can modify the lithium deposition dynamics to form a smooth surface without sharp nuclei for a superior cycling performance of 500 cycles (1000 working hours).

## 2. Results and discussion

SEM images of the Cu-fabric and a single Cu fiber in the fabric were shown in Fig. 1b and c, where each cloth fiber was well coated by a thin copper layer with the interweaved structure reserved. The two red arrows in Fig. 1c marked near a small region of imperfect coating help illustrate the Cu coating layer and the underlying cloth fiber, respectively. The fiber is around 10 μm diameter and the distance between fibers is less than 2 μm. The elastic modulus of the interweaved fabric was measured to show a compressibility around $1.5 \times 10^{-7}$ m/N in Fig. S1. The Cu-fabric framework thus serves as a container with soft cushion that regulates the lithium deposition. The 3D Cu-fabric is further optimized for battery operation under external stresses as will be discussed in detail. The lithium is mostly deposited into the soft Cu-fabric with flat regions distributed uniformly on the surface during the plating and striping processes (Scheme 1), leaving a well-reserved wave-shaped surface pattern. On the contrary, dendrites grow quickly on the 2D Cu foil and penetrates through the Celgard separator. The assembled Li||3D Cu battery also shows a stable cycling performance at high current density and area capacity. The symmetric battery based on lithium deposited on Cu-fabric (Li@Cu-fabric) shows a much more stable performance than the 2D Cu (Li@2D bare Cu).

Li||Cu batteries were assembled in a Swagelok cell configuration to evaluate the electrochemical performance of 2D/3D current collectors. Swagelok cell naturally applies the pressure to the battery electrode configuration by tightening the nuts of the Swagelok battery assembly. 3D Cu-fabric is sensitive to such pressure, since it is a soft substrate with porous and regular microstructures. In order to choose the optimal pressure for battery tests, different external pressures were applied on the battery by tightening the nuts of Swagelok cell with fingers only first, followed by a further screwing using the wrench at 0, 90 and 180°, respectively. Our mechanical property test on the 3D Cu-fabric shows that at 90° the equivalent external pressure applied by the Swagelok cell to the fabric is on the order of 1.0 MPa. Fig. 2a shows that at 1 mA h/cm$^2$ area capacity and 2 mA/cm$^2$ current density the Coulombic efficiency (CE) of the battery cycling shows different performances at different cell pressures. The batteries under 90°' and 180°' pressure show higher initial CE (~90%) than the 0°'s one (<85%). Comparison of the SEM images of lithium deposition under 0°'s (Fig. 2b) and over 90°' pressure (Fig. 2c) after 20 cycles shows that the deposited lithium is more porous without enough pressure, which would likely consume much more electrolyte to cause the faster failure upon cycling. We also find that the 90°' pressure gives the best cycling performance for over 200 cycles, while with increased pressure at 180°, the batteries fail more quickly. As shown in Fig. S2, the holes of Celgard were filled by lithium particles when too high pressure was applied (>240°), which damages the separator and causes the battery failure at the very beginning of the cycling test. Similar but weaker effect can happen at 180° to shorten the cycle life. As a result, screwing the Swagelok cell to 90° is the optimized condition in our tests for the battery cycling performance.

To observe how the 3D Cu-fabric can influence the lithium deposition morphology, scanning electron microscopy (SEM) images of 2D/3D current collectors after the 10th plating were collected, using Swagelok cell with 90°' pressure (Fig. 2d, e). There is a significant difference between the 2D and 3D current collectors. On the 2D bare Cu surface, the lithium deposited inhomogeneously with 3D-like morphology of many nuclei and holes, which is more likely to induce the dendrite growth. In contrast, the lithium deposition onto soft 3D Cu-fabric substrate was more homogeneous with the 2D-like flat morphology (Fig. 3e). No sharp protruding area was observed on the surface of 3D Cu current collector. The results indicate that 3D soft Cu-fabric has the potential to modify the morphology of the lithium deposition for an improved cycling performance.

To further investigate the lithium deposition processes on 2D and 3D Cu current collectors, Li||Cu batteries were assembled to run for 10/50/100 cycles at 2 mA/cm$^2$ current density with 1 mA h/cm$^2$ area capacity. After the last plating, the batteries were disassembled, and the current collectors were studied with SEM. First, on a small scale around 10 μm the deposited lithium shows the separated flat droplet pattern after 10cycles. At 50cycles, some droplets merged together, connected by the "bridge" region (Fig. 3b red dash line). After 100 cycles, the flat regions formed by lithium droplets grew larger to around hundreds of μm (Fig. 3c dash line area). From the cross-section view of 3D current collector after deposition (Fig. S3), most of the deposited lithium was inserted into the Cu-fabric, while the surface of the current collector is always smooth. On the contrary, the lithium deposition on the 2D bare Cu shows much sharper morphologies throughout battery cycling at the same scale in Fig. 3d-f. The comparison between 2D/3D current collectors is more obvious on a large scale around 100 μm. With the 3D soft Cu-fabric, the

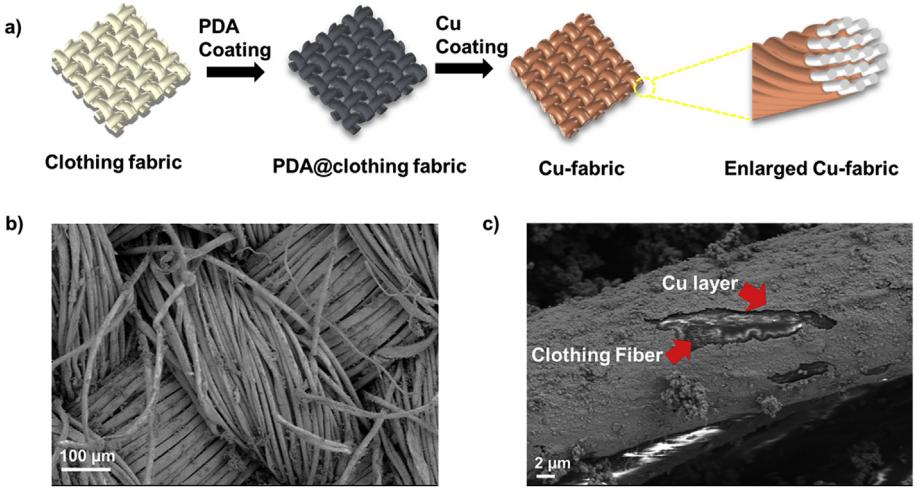


**Fig. 1.** (a) Schematic of 3D Cu-fabric current collector preparation by a two-step dip-coating method. (b) and (c) The SEM imaging of as-prepared Cu-fabric and one magnified fiber of such Cu-fabric.

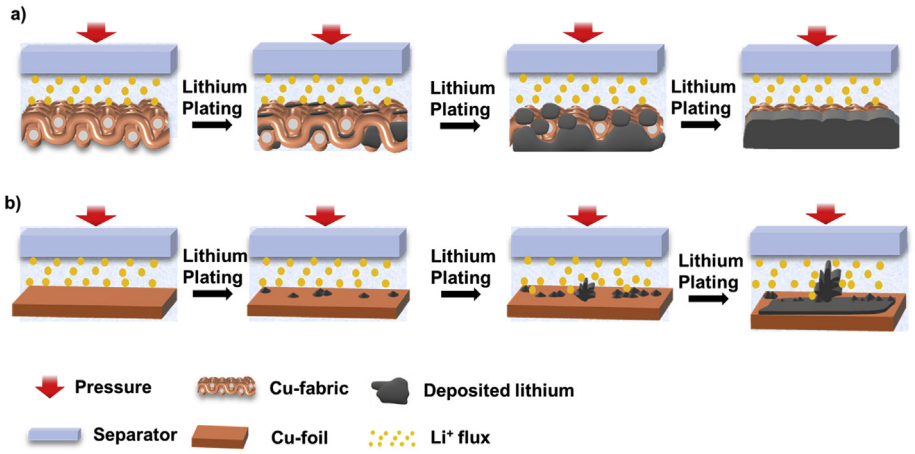


**Scheme 1.** Lithium deposition during lithium plating processes on (a) 3D Cu-fabric and (b) 2D bare copper foil.

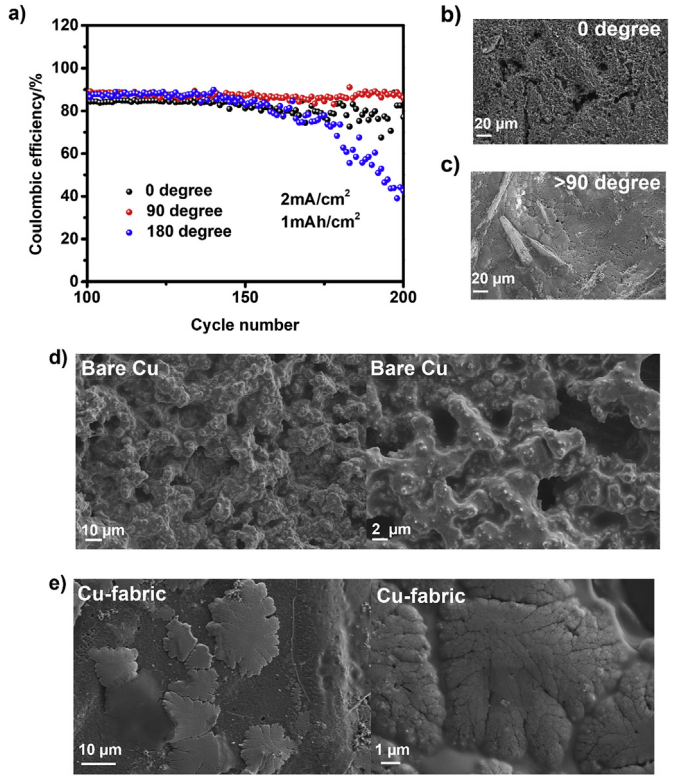


**Fig. 2.** (a) Coulombic efficiency versus cycle number of lithium plating/striping on 3D Cu-fabric under different pressures applied by tightening the nut of Swagelok batteries with 0, 90 and 180°. (b,c) SEM images of the morphology of the lithium deposition after 20th plating under different pressures of (b) 0° and (c) over 90°. (d,e) SEM images of the morphology of the lithium deposition after 10th plating on (d) bare 2D copper and (e) 3D Cu-fabric. (Current density: 2 mA/cm$^2$, area capacity: 1 mA h/cm$^2$).

deposited lithium surface on the current collector was uniformly and densely distributed. Note that the wave pattern of the underlying fabric remained after 100 cycles, although it becomes weaker upon cycling. However, on 2D Cu the deposited lithium shows various kinds of inhomogeneous morphologies during the cycling. According to these results, the 3D Cu-fabric regulates the shape of the deposited lithium throughout the hundreds of lithium plating and stripping processes for the improved cycling performance.

We now try to elucidate one major aspect of the mechanism that is underlying the observed mechanical and electrochemical interactions. As discussed above, the SEM pictures show the lithium deposition inside the fabric and on the surface. At the beginning of the lithium deposition, bulk lithium must squeeze into the porous region inside the fabric due to the volume constriction applied by the external pressure. Two resistance forces in this process, as illustrated in Fig. 4a, are the surface tension pressure $p_\sigma = 2\alpha/s$ ($\alpha$ is the surface tension coefficient of Li metal at room temperature), assuming a curved surface of the squeezed-in lithium, and the friction $f$ between the squeezed-in lithium and the cloth fibers, which is proportional to the number of fiber layers, $N$, that the lithium has penetrated. This squeezed-in process must stop when the resistance forces grow larger than the external pressure. Since the mobility of Li metal is limited, this process is limited by kinetics. Thus, there is simultaneous plating of Li metal along with such squeezing effect (Fig. 4a).

As was revealed by our experiments, the Cu fabric shows much better ability to suppress a critical step in the lithium dendrite formation, i.e., the trunk growth of lithium [31]. As shown in Fig. 4b, because the modulus of Li (4.9 GPa) is much larger than the modulus of the separator ($\ll$ 1 GPa), for bare Cu with a hard Cu substrate, the Li trunk induced pressure $\Delta p$ cannot reshape the Li trunk. Thus, with growing Li trunk, the deformation of the separator and extra local pressure are also accumulating, leading eventually to the crack or penetration of the separator. On the contrary, in the Cu-fabric case, because of the porous gap region between the fibers, the extra local pressure induced by any Li trunk growing toward the separator can be effectively relieved through a deformation of bulk lithium into the porous 3D fibric, as well as spreading out on the surface. For more significant trunk growth with larger $\Delta p$, the extra pressure at the bottom, $\Delta p'$, $\Delta p''$ and $\Delta p'''$, etc., are also larger. Thus, the porous nature of the cloth provides a robust negative feedback that prevents the growth of Li trunks.

Quantitatively, the key force balance is expressed as:

$$p_{ext} \cdot s = Nf + p_\sigma \cdot s.$$

Suppose the compressibility $\beta = -\frac{1}{V}\frac{dV}{dp}$ is a constant under the experiment conditions, we have

$$V_{pore} = V_0 e^{-\beta p_{ext}}$$

where $V_0$ is the original volume of the pores under zero pressure. Suppose the cloth fibers have a cylinder shape along $y$ direction (Fig. 4a), $V_{pore}$ is proportional to $s^2$. Also, because the total volume of Li penetration inside the cloth per unit length in $y$ direction is $V_{in\_cloth} = kN \cdot s^2$ ($k \approx 1$), assuming the friction $f$ is also a constant, we can write the equilibrium formula for $V_{in\_cloth}$,

$$V_{in\_cloth} f = p_{ext} s_0^3 e^{-\frac{3\beta p_{ext}}{2}} - \alpha s_0^2 e^{-\beta p_{ext}}$$

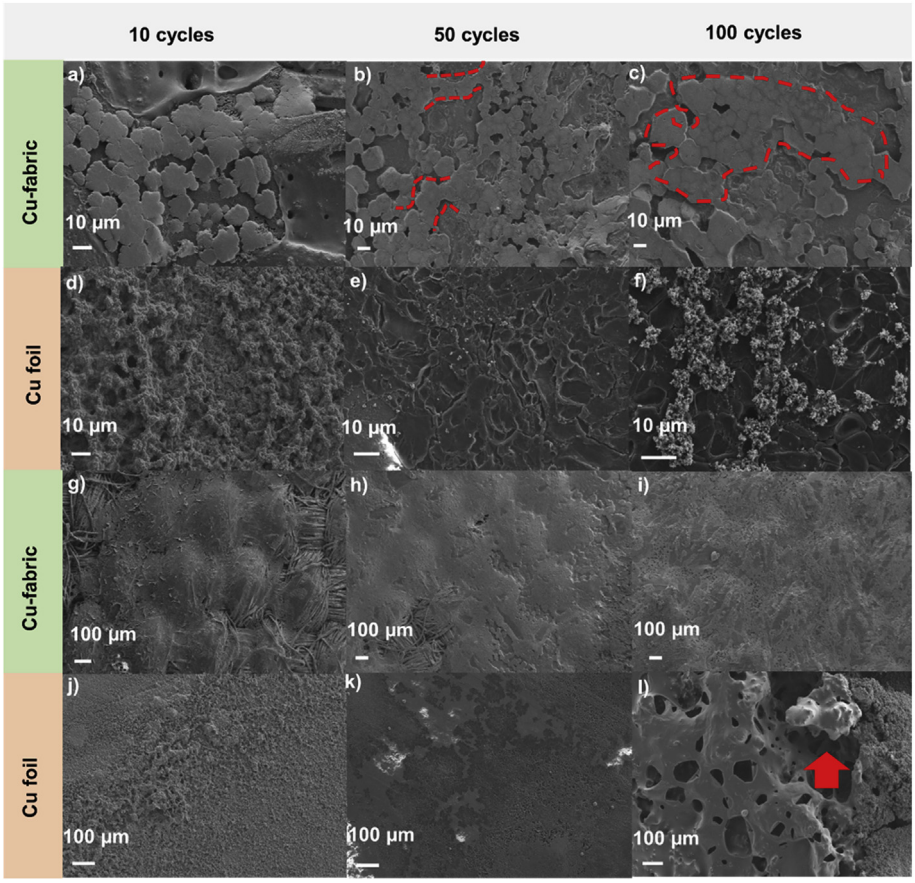


**Fig. 3.** Scanning electron microscopy imaging of the morphology of lithium deposition after (a, d, g, j) 10th, (b, e, h, k) 50th and (c, f, i, l) 100th plating on (a-c, g-i) 3D Cu-fabric and (d-f, j-l) 2D bare Cu. (a-f) the scale bar is 10 μm; (g-l) the scale bar is 100 μm.

Interestingly, this equation predicts an optimal external pressure that maximizes $V_{in\_cloth}$, which is

$$p_{ext}^{opt} = \frac{2}{3\beta} + \frac{2\alpha e^{1/3}}{3s_0}$$

as a function of only materials-dependent quantities. Based on the above calculation and the experimental results shown in the figure, we obtained the maximum amount of Li storable inside the fabric as a function of the external pressure, using the experimentally measured compressibility $\beta \approx 1.5 \times 10^{-7}$m/N, average gap size $s_0 \approx 1\mu m$ and friction $f \approx 300$N/m. (Fig. 4c). We predicted an optimal pressure of 4.78 MPa that is reasonably close to the experimentally determined optimal pressure on the order of 1 MPa.

Suppose the porosity of the cloth without pressure is 10% and the thickness and area are 200 μm and 1 cm [2], under the optimal pressure the volume of porous region decreases to about $1/e$, giving a compressed thickness around 74 μm and a total volume inside the cloth as

$$V_{pore} = 0.2 \times 100 \times \frac{0.1}{e} \approx 0.74 \ \ \text{mm}^3$$

while the total volume of Li in one charge or discharge is 0.48 $mm^3$, based on the capacity of 1 mAh/$cm^2$, the electrode area of 1 $cm^2$ and the volumetric capacity of 2061 mAh/$cm^3$, corresponding to around 65% thickness of the compressed fabric, or 48 μm thick, in an ideal situation of homogeneous and dense lithium propagation inside the 3D structure with porosity of 10% [40]. Thus, for the 200 μm thick fabric sample we used, it's not surprising to see the Li penetration almost to the other side of the fabric (SI Fig. S3). Based on our model, increasing the porosity of the cloth and decreasing its compressibility are two ways to increase the Li capacity inside the fabric (Fig. 4d). For example, if the fabric is made with 20% porosity and a compressibility 10 times smaller than our cloth, all deposited lithium metal can be in principle submerged inside the fabric with only 24 μm thickness, corresponding to around only 12% of the compressed thickness for a much more enhanced redundancy in lithium storage capacity inside the 3D cloth. As illustrated in Fig. 4d, smaller compressibility and larger porosity is thus preferred. However, too large porosity leads to a weaker interaction between the 3D structure and the deposited Li, as previously discussed in the case of 3D Cu wires [38], where structure modulated charge density plays a major role there. While with reduced porosity in the 3D fabrics, stronger interaction between the 3D structure and the deposited Li is expected (Fig. 4d).

We also tested the electrochemical performance of fabrics with different materials and thicknesses after Cu coating (Fig. S4). The Cu-fabric based on polyester (784 μm) and silk (128 μm) both showed over 300 stable cycles at 1 mA/$cm^2$ current density and 1 mA h/$cm^2$ area capacity, which suggests a large flexibility in materials, structures and especially, thicknesses of the Cu coated fabrics for the battery application. Current lithium ion batteries utilize graphite as anode with a specific capacity of 719 mA h/$cm^3$, versus the lithium metal capacity of 2061 mA h/$cm^3$. The utilization of lithium metal can in principle largely reduce the volume of anode. In an ideal case, for the battery with 3.28 mA h/$cm^2$ capacity (area loading for commercial battery), the thickness of deposited lithium metal is about 16 μm. In contrast, about 70 μm thick graphite is required for a lithium ion battery, taking account of the porosity of anode. Therefore, as long as the thickness of the 3D copper current collector is less than 54 μm, the volumetric density of lithium metal battery is higher than lithium ion battery with graphite as anode [40]. Note that these fabrics we used are all commercially available cloth textures, while based on the mechanism understanding from

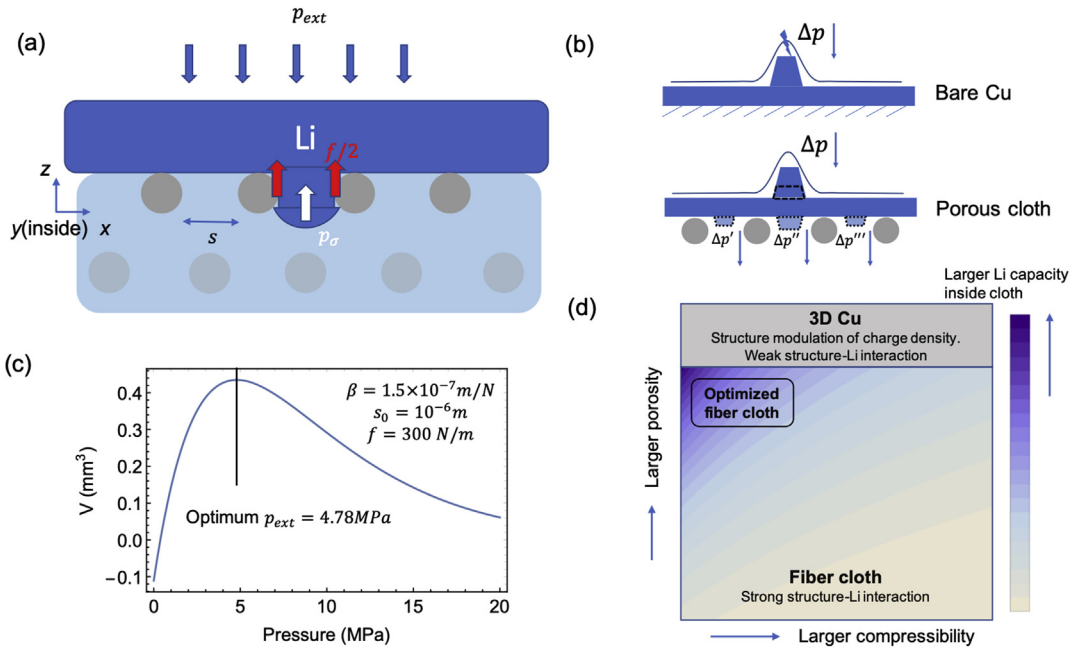


**Fig. 4.** Modelling lithium deposition under external pressure. (a) Schematic illustration of our model. $p_{ext}$ and $p_\sigma$ are the external pressure and the surface tension pressure, respectively. $f$ is the total friction on the lithium exerted by each layer of cloth. (b) Illustration of the suppression of Li trunk and more even distribution of Li observed in experiments. (c) The maximum volume of lithium that can be stored in the fabric as a function of external pressure, with experimentally measured compressibility $\beta \approx 1.5 \times 10^{-7}$m/N, average fiber gap size $s_0 \approx 1\mu m$ and friction $f \approx 300$N/m. The predicted optimal external pressure of 4.78 MPa is reasonably close to the experimental value on the order of 1.0 MPa. (d) Schematic illustration of the performance of structured current collector in the compressibility and porosity space. Darker blue is the region with larger lithium storage capacity inside the 3D Cu-fabric structure. (For interpretation of the references to color in this figure legend, the reader is referred to the Web version of this article.)

our model analysis it is possible to further design a fabric with optimized structural parameters to achieve better performances with much smaller thickness than 100 μm.

Li||Cu batteries were also applied to test the long-cycle electrochemical performance of the 3D Cu-fabric electrode. Lithium was deposited to the 3D/2D current collectors, then the battery cycled by discharging with capacity of 1 mA h/cm$^2$ and then charging to a cut-off voltage at 0.5V, at 1 mA/cm$^2$ or 2 mA/cm$^2$ current density. The Coulombic efficiency (CE) versus cycle numbers is the main parameter we focused on here to evaluate the cycling stability. When CE decreases quickly or shows large fluctuations, it usually means that lithium dendrite growth is out of control and the battery approaches the failure. The CEs of lithium stripping/plating process on 2D/3D current collectors were shown in Fig. 5a-c at various current density and area capacity. In Fig. 5a, the CE of 3D Cu-fabric electrode maintains to be stable over 90% for 500 cycles or1000 h at 1 mA/cm$^2$ current density and 1 mA h/cm$^2$ area capacity. On the contrary, the CE of 2D bare Cu electrode dropped to be less than 80% quickly after about 60 cycles. It is obvious that the 3D Cu-fabric shows a much longer cycle life. The battery, however, shows a sudden increase of overpotential after 500 cycles, as depicted in Fig. S5, which can be attributed to the consumption of electrolyte after such long cycle [41]. The battery was stopped and disassembled after it shows such irregular overpotential curve, and the surface morphology was characterized for the 3D Cu-fabric. No obvious nucleation existed on the electrode surface and the surface shape of the fibric was still maintained, suggesting that the 3D Cu-fabric regulated the lithium deposition into the fiber and reduced the damage to the separator. At higher current density of 2 mA/cm$^2$, batteries with 3D Cu-fabric current collector still cycled over 200 cycles while the battery with 2D bare Cu current collector failed after 30 cycles (Fig. 5b). The corresponding impedance is measured before and after battery cycles. The interface resistance, represented by the half-circuit in Fig. S6, shows a small level of increase. This growth of interface resistance is due to the formation of SEI. It, however, doesn't show a very quick growth of resistance after 200 cycles. At higher area capacity of 2 mA h/cm$^2$, 3D Cu-fabric electrode battery maintained a CE over 90% for 100 cycle or 400 h. Under the same test condition, 2D bare Cu electrode battery short-circuited after 60 cycles or 240 h (Fig. 5c). Comparing the CE performance between 2D/3D Cu current collectors, the 3D Cu-fabric greatly improved the stability of lithium metal anode. These results are consistent with our model simulation and SEM images of morphology as shown in Figs. 2-4. The Coulombic efficiency can also influenced by the choice of electrolyte. Note that to get higher coulombic efficiency, ether-based electrolyte with additive was tested to show an increased CE over 97% with stable cycling over 90 cycles (Fig. S7).

Li@Cu||Li@Cu symmetric batteries were also used for testing the stability of electrodes (Fig. 5d). The lithium was firstly deposited to the 2D/3D Cu current collectors and then collected to assemble the symmetric batteries. The batteries were cycled at a high current density of 2 mA/cm$^2$, and discharge or charge for 30min in each half cycle. The polarization of Li@3D Cu-fabric battery (≈0.1V) is much smaller than that of Li@2D bare Cu battery (≈0.2V) for the first several cycles. After 50cycles, the Li@3D Cu-fabric battery was still stable, while the Li@2D bare Cu battery showed large polarizations. Based on the comparison of electrochemical performances between 2D and 3D Cu-fabric current collectors, 3D Cu-fabric electrode shows great promise to achieve a more stable lithium deposition on the anode at higher current density. Therefore, we suggest that the soft Cu-fabric structure made by our dip-coating method could be an effective 3D conductive framework for improving the safety performance of lithium metal anode batteries, which is applicable to a broad choice of pristine materials and flexible design of 3D structures with tunable geometries and mechanical properties.

## 3. Conclusion

In this work, we developed a soft 3D Cu-fabric current collector, which achieved superior long-cycle performance with the commercial carbonate electrolyte. Combining experimental and simulation results,

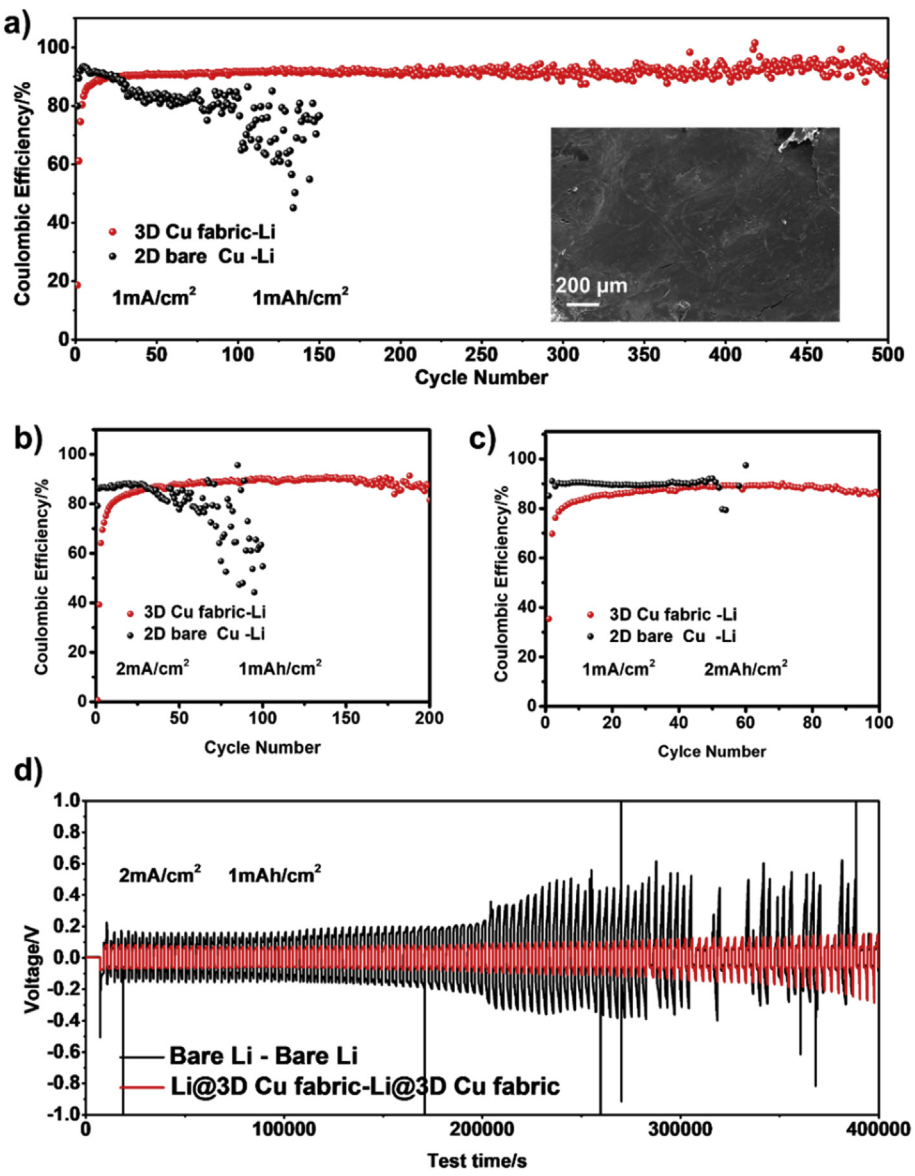


**Fig. 5.** Coulombic efficiency of lithium striping/plating on 2D bare copper and 3D Cu-fabric substrate under different current density and area capacity. (electrolyte: EC/DEC=1:1,1 M $LiPF_6$). (a) 1 mA/cm$^2$ and 1 mA h/cm$^2$. Inset: SEM image of the fabric after battery failure. (b) 2 mA/cm$^2$ and 1 mA h/cm$^2$. (c) 1 mA/cm$^2$ and 2 mA h/cm$^2$. (d) Voltage-time profiles of the lithium stripping/plating process with 2 mA/cm$^2$ current density and 1 mA h/cm$^2$ area capacity in Li||Li(black) and Li@Cu-fabric ||Li@Cu-fabric (red) symmetric batteries. (For interpretation of the references to color in this figure legend, the reader is referred to the Web version of this article.)

we suggested an optimal external pressure to the battery operation, by considering the strong interaction between the deposited lithium and the Cu-fabric structure in the squeezing and flattening processes during the battery stripping and plating cycles. The 3D Cu-fabric surface maintained to be smooth without obvious dendrite growth after cycling. Simulations were also performed to understand the mechanism with a design principle proposed for such 3D-structured current collectors. The 3D Cu fabric herein is prepared from cloth fiber with a scalable dip-coating method, which makes it compatible with large-scale industrial test and production. Our method is thus powerful in a high-throughput design, search and test of next generation 3D anodes for lithium metal battery applications.

## 4. Experimental section

*Fabrication and Characterization of 3D Cu-fabric*: The framework of the current collector is collected from lab clothing. The composition of the clothing fabric is 80% polyester and 20% cotton. Cu-fabric was prepared by a two-step dip-coating method: first of all, the clothing fabric was soaked into 2 mg/ml dopamine solution (dissolved in PH=8.5, 0.01 M Tris-HCL buffer) for 48 h under room temperature. Then the polydopamine (PDA) coated clothing fabric (PDA@clothing fabric) was collected by washing three times with distilled water. Second, the PDA@clothing fabric was dipped into $CuCl_2$ aqueous solution (0.05 M $CuCl_2$, 0.05 M ethylenediaminetetraacetic acid, 0.1 M $H_3BO_3$, NaOH, pH=7), and 0.1 M dimethylamine-borane was added as the reducing agent. This step was performed at room temperature for 24 h until the solution was colorless and the fabric was covered by a thin copper layer. The Cu-fabric was rinsed by distilled water for three times and then dried at 90 °C. The morphology of Cu-fabric was characterized by SEM. The mechanical properties of the Cu fabric were measured by a material testing machine (Instron, USA).

*Electrochemical Measurement*: Swagelok cell structure was utilized for all the battery assemblies. To optimize the external pressure for the battery test, different levels of pressures were applied during the battery assemble by screwing the Swagelok tightly until different degrees. To test the Coulombic efficiency, 3D Cu-fabric or 2D bare Cu was used as the working electrode, lithium foil as the counter electrode and Celgard 2325 as the separator. The electrolyte is 1 M hexafluorophosphate ($LiPF_6$) in ethylene carbonate (EC) and diethyl carbonate (DEC), EC/DEC=50/50 (v/v), battery grade. All the batteries were assembled in argon filled glove-box. The battery tests were performed on a LAND cell test

instrument. After rest for 1 h, 1 mA h/cm$^2$ lithium was deposited to 3D/2D current collectors and then the batteries were cycled with 1 mA/cm$^2$ or 2 mA/cm$^2$. Higher area capacity (2 mA h/cm$^2$) of deposited lithium was also applied in this system. The morphologies of the lithium deposition on 3D/2D current collectors were characterized by scanning electron microscope. During the symmetric cell test, 6 mAh lithium was deposited on the 3D/2D current collectors and then the batteries were discharged/charged at 2 mA/cm$^2$ for 30min in each half cycle. The voltage-time profile was collected.

## Declaration of competing interest

The authors declare no conflict of interest.

## Acknowledgements

This work was supported by Dean's Competitive Fund for Promising Scholarship at Harvard University. The SEM experiments were conducted at the Center for Nanoscale Systems (CNS) at Harvard University supported by the National Science Foundation.

## Appendix A. Supplementary data

Supplementary data to this article can be found online at https://doi.org/10.1016/j.ensm.2019.11.007.

## References

[1] X.B. Cheng, R. Zhang, C.Z. Zhao, Q. Zhang, Toward safe lithium metal anode in rechargeable batteries: a review, Chem. Rev. 117 (2017) 10403–10473.
[2] M.D. Tikekar, S. Choudhury, Z. Tu, L.A. Archer, Design principles for electrolytes and interfaces for stable lithium-metal batteries, Nat. Energy 1 (2016).
[3] D. Lin, Y. Liu, Y. Cui, Reviving the lithium metal anode for high-energy batteries, Nat. Nanotechnol. 12 (2017) 194–206.
[4] J. Liu, et al., Pathways for practical high-energy long-cycling lithium metal batteries, Nat. Energy 4 (2019).
[5] A. Zhamu, et al., Reviving rechargeable lithium metal batteries: enabling next-generation high-energy and high-power cells, Energy Environ. Sci. 5 (2012) 5701–5707.
[6] K.J. Harry, D.T. Hallinan, D.Y. Parkinson, A.A. MacDowell, N.P. Balsara, Detection of subsurface structures underneath dendrites formed on cycled lithium metal electrodes, Nat. Mater. 13 (2014) 69–73.
[7] S. Li, et al., Developing high-performance lithium metal anode in liquid electrolytes: challenges and progress, Adv. Mater. 30 (2018) 1706375.
[8] T. Jaumann, et al., Role of 1,3-dioxolane and LiNO 3 addition on the long term stability of nanostructured silicon/carbon anodes for rechargeable lithium batteries, J. Electrochem. Soc. 163 (2016) A557–A564.
[9] X.Q. Zhang, et al., Highly stable lithium metal batteries enabled by regulating the solvation of lithium ions in nonaqueous electrolytes, Angew. Chem. Int. Ed. 57 (2018) 5301–5305.
[10] X. Fan, et al., Non-flammable electrolyte enables Li-metal batteries with aggressive cathode chemistries, Nat. Nanotechnol. 13 (2018) 1–8.
[11] E. Markevich, G. Salitra, F. Chesneau, M. Schmidt, D. Aurbach, Very stable lithium metal stripping–plating at a high rate and high areal capacity in fluoroethylene carbonate-based organic electrolyte solution, ACS Energy Lett. 2 (2017) 1321–1326.
[12] X.Q. Zhang, X.B. Cheng, X. Chen, C. Yan, Q. Zhang, Fluoroethylene carbonate additives to render uniform Li deposits in lithium metal batteries, Adv. Funct. Mater. 27 (2017).
[13] X.B. Cheng, et al., Implantable solid electrolyte interphase in lithium-metal batteries, Chem 2 (2017) 258–270.
[14] Q. Pang, X. Liang, A. Shyamsunder, L.F. Nazar, An in vivo formed solid electrolyte surface layer enables stable plating of Li metal, Joule 1 (2017) 871–886.
[15] Q. Li, S. Zhu, Y. Lu, 3D porous Cu current collector/Li-metal composite anode for stable lithium-metal batteries, Adv. Funct. Mater. 27 (2017).
[16] D. Wang, et al., Zipper-inspired SEI film for remarkably enhancing the stability of Li metal anode via nucleation barriers controlled weaving of lithium pits, Adv. Energy Mater. 8 (2018).
[17] E. Quartarone, P. Mustarelli, Electrolytes for solid-state lithium rechargeable batteries: recent advances and perspectives, Chem. Soc. Rev. 40 (2011) 2525–2540.
[18] X.B. Cheng, et al., A review of solid electrolyte interphases on lithium metal anode, Adv. Sci. 3 (2015).
[19] Y. Li, et al., Atomic structure of sensitive battery materials and interfaces revealed by cryo–electron microscopy, Science 80 (358) (2017) 506–510.
[20] B. Zhu, et al., Poly(dimethylsiloxane) thin film as a stable interfacial layer for high-performance lithium-metal battery anodes, Adv. Mater. 29 (2017).
[21] C. Yan, et al., Dual-layered film protected lithium metal anode to enable dendrite-free lithium deposition, Adv. Mater. 30 (2018) 1707629.
[22] R. Xu, et al., Artificial soft–rigid protective layer for dendrite-free lithium metal anode, Adv. Funct. Mater. 28 (2018).
[23] L. Li, et al., Self-heating–induced healing of lithium dendrites, Science 80 (359) (2018) 1513–1516.
[24] G. Zheng, et al., Interconnected hollow carbon nanospheres for stable lithium metal anodes, Nat. Nanotechnol. 9 (2014) 618–623.
[25] E. Cha, et al., 2D MoS2 as an efficient protective layer for lithium metal anodes in high-performance Li–S batteries, Nat. Nanotechnol. 13 (2018) 337–344.
[26] Y. Wu, et al., A room-temperature liquid metal-based self-healing anode for lithium-ion batteries with an ultra-long cycle life, Energy Environ. Sci. 10 (2017) 1854–1861.
[27] P. Zou, et al., Directing lateral growth of lithium dendrites in micro-compartmented anode arrays for safe lithium metal batteries, Nat. Commun. 9 (2018).
[28] H. Zhao, et al., Compact 3D copper with uniform porous structure derived by electrochemical dealloying as dendrite-free lithium metal anode current collector, Adv. Energy Mater. 8 (2018) 1–8.
[29] R. Zhang, et al., Advanced micro/nanostructures for lithium metal anodes, Adv. Sci. 4 (2017).
[30] C.P. Yang, Y.X. Yin, S.F. Zhang, N.W. Li, Y.G. Guo, Accommodating lithium into 3D current collectors with a submicron skeleton towards long-life lithium metal anodes, Nat. Commun. 6 (2015).
[31] L. Liu, et al., Free-standing hollow carbon fibers as high-capacity containers for stable lithium metal anodes, Joule 1 (2017) 563–575.
[32] P. Bai, J. Li, F.R. Brushett, M.Z. Bazant, Transition of lithium growth mechanisms in liquid electrolytes, Energy Environ. Sci. 9 (2016) 3221–3229.
[33] X. Wang, et al., Stress-driven lithium dendrite growth mechanism and dendrite mitigation by electroplating on soft substrates, Nat. Energy 3 (2018) 227–235.
[34] T. Hirai, Influence of electrolyte on lithium cycling efficiency with pressurized electrode stack, J. Electrochem. Soc. 141 (1994) 611.
[35] C. Monroe, J. Newman, The impact of elastic deformation on deposition kinetics at lithium/polymer interfaces, J. Electrochem. Soc. 152 (2005) A396.
[36] C. Monroe, Newman, J. Dendrite growth in lithium/polymer systems, J. Electrochem. Soc. 150 (2003) A1377.
[37] H.J. Chang, et al., Investigating Li microstructure formation on Li anodes for lithium batteries by in situ $^6$Li/$^7$Li NMR and SEM, J. Phys. Chem. C 119 (2015) 16443–16451.
[38] L.Y. Qi, et al., A versatile strategy to fabricate 3D conductive frameworks for lithium metal anodes, Adv. Mater. Interfaces 5 (2018).
[39] H. Lee, S.M. Dellatore, W.M. Miller, P.B. Messersmith, Mussel-inspired surface chemistry for multifunctional coatings, Science 80 (318) (2007) 426–430.
[40] A.J. Louli, et al., Exploring the impact of mechanical pressure on the performance of anode-free lithium metal cells, J. Electrochem. Soc. 166 (2019) A1291–A1299.
[41] X. Chen, L. Ye, Y. Wang, X. Li, Beyond-expert-level performance prediction for rechargeable batteries by unsupervised machine learning, Adv. Intell. Syst. (2019), 1900102, 1900102.